ESTABLISHMENT AND PARAMETER CALIBRATION OF QUINOA SEED-SOIL CONTACT MODEL BASED ON DISCRETE ELEMENT METHOD
/
基于离散元法的藜麦种子-土壤接触模型建立及参数标定

Wenxue DONG, Xuan ZHAO, Fei LIU*), Hongbin BAI, Dezheng XUAN, Anbin ZHANG, Yuxing REN
College of Mechanical and Electrical Engineering, Inner Mongolia Agricultural University, Hohhot 010010, China;
Tel: 13238446338; E-mail: dong18403045597@163.com; afei2208@imau.edu.cn
DOI: https://doi.org/10.35633/inmateh-76-75

Keywords: *Parameter calibration; Quinoa seed-soil; Contact model; Dynamic angle of repose*

ABSTRACT
This study provides valuable insights into the interaction between seeds and soil, specifically focusing on quinoa seeds. Accurate discrete element contact models and parameters have been lacking in this area, which has somewhat hindered the optimization and improvement of seeders. By analyzing the collision process between quinoa seeds and soil through contact experiments, the study finds that the adhesive force of the soil on quinoa seeds is much greater than the gravitational force on the seeds and increases with higher soil moisture content. The load-displacement curve obtained from the experiments closely resembles the loading-displacement curve of the JKR (Johnson-Kendall-Roberts) model, leading to the selection of the JKR contact model for simulating the quinoa seed-soil mixture. Using Plackett-Burman experiments, the study identifies the key factors that significantly affect the dynamic angle of repose: soil surface energy, quinoa seed-soil surface energy, and the static friction coefficient between quinoa seeds and soil. Based on the principles of Box-Behnken experimental design, regression analysis and parameter optimization are conducted on these significant factors, resulting in optimal parameter combinations under varying soil moisture content. The verification experiment shows an error of within 1.9%, demonstrating the accuracy of the calibrated parameters. This research provides a solid theoretical foundation for discrete element simulation of seed-soil contact, offering a reference for improving the design and efficiency of seeders.

摘要
种子-土壤相互作用的研究中缺乏准确的离散元接触模型和参数，在一定程度上限制了播种机具的优化改进。本文以藜麦种子与土壤为研究对象，通过接触试验分析藜麦种子与土壤接触碰撞过程，发现土壤对藜麦种子的粘附力远大于种子重力并随土壤含水率的增加而增加。试验所得加载位移曲线与 JKR 模型加载位移曲线规律相似，因此选用 JKR 接触模型作为藜麦种子-土壤混料接触模型。通过 Plackett-Burman 试验筛选出了对动态休止角影响显著的因素。通过 Box-Behnken 试验得到了不同土壤含水率下的较优参数组合。验证试验误差在 1.9%以内，证明了标定参数的准确性。这为种子与土壤接触的离散元仿真提供了理论参考。

INTRODUCTION
The balanced distribution of nutrients and water in the soil is crucial for crop growth (*Cay et al., 2018*), while uniform seed spacing in the field directly influences crop yield (*Pareek et al., 2023; Sun et al., 2022*). However, the actual grain spacing achieved by precision seeders in field operations often deviates from uniformity due to accumulated errors (*Abdolahzare et al., 2018; Xie et al., 2023; Liu et al., 2022*). One significant factor affecting seed spacing uniformity is the seed bounce displacement caused by the impact of seeds with the soil in the seed furrow during their release from the seed metering device (*Li et al., 2022; Yan et al., 2020*). Thus, a comprehensive and systematic investigation into the mechanisms of seed-soil contact collision and the key factors influencing seed bounce displacement is essential. Such research holds substantial theoretical and practical importance for enhancing seed spacing uniformity. Physical experiments studying seed-soil collision processes are heavily influenced by seasonal climate conditions, making it challenging to obtain accurate measurements of parameters like collision contact force, collision speed, and bounce displacement. These parameters are critical for the design and optimization of seed metering devices. The discrete element method (DEM), a numerical simulation technique, offers an effective solution for examining seed-soil contact and collision processes (*Lei et al., 2021; Liao et al., 2023*).

Before conducting DEM simulation tests, it is necessary to establish a discrete element contact model and calibrate corresponding contact parameters (e.g., collision restitution coefficient, static friction coefficient, dynamic friction coefficient, surface energy) (*Zhao et al., 2022*).

Research to date has successfully calibrated DEM simulation parameters for various seeds, including corn (*Liu et al., 2021; Wang et al., 2016; Shi et al., 2023*), rice (*Zhang et al., 2020*), wheat (*Horabik et al., 2020; Sun et al., 2022*), and notoginseng (*Yu et al., 2020*). Findings suggest that the Hertz-Mindlin (no-slip) contact mechanics model is particularly suitable for calibrating parameters of dry seed particles, although contact parameters vary significantly between different seed types. During the sowing period, soil moisture content typically ranges from 15% to 20%, which introduces a degree of adhesion (*Wang et al., 2021*). To address this, many researchers use models like the Johnson-Kendall-Roberts (JKR) model (*Yang et al., 2024*), the Edinburgh Elasto-Plastic Adhesive (EEPA) model (*Chen et al., 2023*), or the Hertz-Mindlin with Bonding model (*Song et al., 2022; Zhou et al., 2023*) for soil parameter correction. However, modeling seeds or soil independently does not accurately reflect the seed-soil contact and collision dynamics, emphasizing the need for a suitable seed-soil mixture contact model.

Mixture contact models are crucial for accurately describing interactions between different particles and understanding the interaction mechanisms (*Zhang et al., 2023; Fang et al., 2022; Jiang et al., 2023*). These models are generally categorized into non-viscous and viscous contact models. Non-viscous models, such as the Hertz-Mindlin (no-slip) model, are typically used for dry particles (*Liao et al., 2022*). For mixtures involving viscous particles, models like JKR and EEPA are more appropriate (*Ma et al., 2022; Tian et al., 2021*). Although there has been progress in developing mixture contact models, theoretical research, particularly regarding model selection, remains insufficient (*Walunj et al., 2023*). For instance, *Zhou et al.* (*2023*) used the EEPA model to calibrate parameters for soil cohesion in a corn seed-soil contact test, highlighting the rationale behind choosing this model. Given the substantial differences in size and shape between quinoa and corn seeds, it remains unclear whether the EEPA model is suitable for smaller seeds like quinoa. Hence, further investigation into the contact models and parameter calibration for small-sized seeds and soil is necessary for accurately studying seed-soil collision during seed placement.

Addressing these issues, this study focuses on quinoa seeds and the specific soil used for quinoa cultivation, examining the contact process between quinoa seeds and soil. It aims to identify the most suitable contact model for quinoa seed-soil mixtures and calibrate relevant contact parameters. This research provides a theoretical foundation for developing contact models for small-sized seeds and offers valuable insights for studying mixture contact collisions.

MATERIALS AND METHODS

Quinoa Seed-soil Contact Test

During sowing, soil typically contains a certain level of moisture. Capillary water between soil particles forms discontinuous liquid bridges, creating adhesion between the particles. However, whether this adhesion force needs to be considered when establishing a collision contact model for small-sized seeds like quinoa and soil requires further investigation.

In this experiment, a texture analyzer was used to study the adhesion of quinoa seeds to soil when the seeds were in vertical contact with the soil, as shown in Figure 1. Six quinoa seeds of similar size (2.15 mm in length, 2.10 mm in width, and 1.28 mm in thickness) were attached to a probe, and soil was placed in a tray. The experiment was conducted with soil moisture content as the test variable. Considering that the ideal soil moisture content for quinoa sowing ranges from 15% to 20%, tests were performed at moisture levels of 15%, 17.5%, and 20%. Each experimental condition was repeated three times for accuracy.

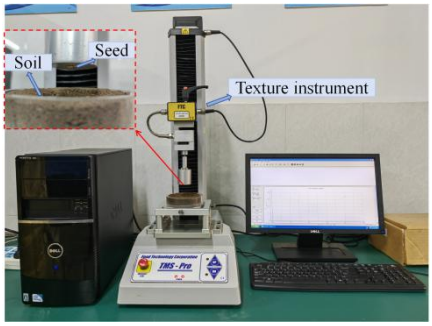

Fig. 1 - Quinoa seed-soil contact test device

During the test, the probe descends vertically at a speed of 30 mm/min. When it comes into contact with the soil, it continues to compress the soil until it reaches 30% deformation. Afterward, it starts the unloading phase, retracting at the same speed of 30 mm/min.

If the adhesion force of the soil on the quinoa seeds is greater than the gravitational force acting on the seeds, it shows that soil adhesion significantly affects the contact and collision dynamics between quinoa seeds and soil. In such cases, the adhesion force should be taken into account when creating a quinoa seed-soil contact model.

Physical Experiment of Quinoa Seed-soil Dynamic Angle of Repose

The dynamic angle of repose refers to the maximum angle between the slope of an accumulated pile of particles and the horizontal plane before the particles begin to collapse. This occurs when the inter-particle forces can no longer balance with gravity during the rotation of the particles within the drum. Figure 2 illustrates a custom-built device for measuring the dynamic angle of repose. This device consists of a drum (200 mm in diameter, 100 mm in length, made of organic glass), a coupling, a motor, and a controller.

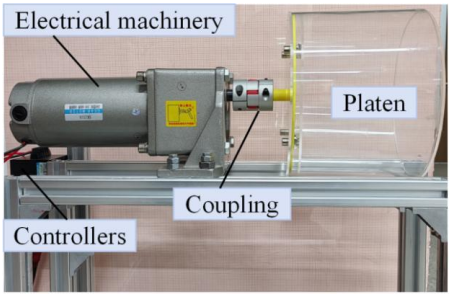

Fig. 2 - Measuring device for dynamic angle of repose

In the experiment, a quinoa seed-soil mixture was prepared with a seed-to-soil ratio of 1:4. The motor speed was set to 20 r/min. Once the speed stabilized, the dynamic angle of repose of the quinoa seed-soil mixture was recorded in real-time. Three experimental groups were established, with soil moisture content set at 15%, 17.5%, and 20% for each group, respectively. Each test was repeated three times, and the average value was taken for analysis.

Simulation Test of Quinoa Seed-soil Dynamic Angle of Repose

(1) JKR Contact Theory

The Hertz-Mindlin with JKR contact model is a cohesive model, whose surface energy can simulate the cohesive force between particles. The model is suitable for simulating wet viscous particles and agglomerated materials. The viscoelastic characteristics between particles can be expressed by the normal elastic force in the model. The normal elastic force is based on the normal overlap and surface energy:

$$F_{JKR} = -4\sqrt{\pi U_S E^*}\, a^{\frac{3}{2}} + \frac{4E^*\alpha^3}{3R^*} \tag{1}$$

$$\gamma = \frac{\alpha^2}{R^*} - \sqrt{\frac{4\pi U_S \alpha}{E^*}} \tag{2}$$

$$\frac{1}{E^*} = \frac{1-\nu_1^2}{E_1} + \frac{1-\nu_2^2}{E_2} \tag{3}$$

$$\frac{1}{R^*} = \frac{1}{R_1} + \frac{1}{R_2} \tag{4}$$

In the formula, F_{JKR} is JKR normal elastic force, N; U_S is the surface energy, (N/m), E^* is the equivalent elastic modulus, Pa; γ is the normal overlap between two contact particles, m; α is the radius of contact circle between two contact particles, mm; R^* is the equivalent contact radius, mm; R_1, R_2 is the contact radius of two particles, mm; ν_1, ν_2 is the Poisson 's ratio of two particles; E_1, E_2 is the elastic modulus of two contact particles, Pa.

When U_S is 0, the normal force of JKR can be simplified to Hertz-Mindlin normal force F_{Hertz}.

$$F_{JKR} = F_{Hertz} = \frac{4E^* \sqrt{R^*} \gamma^{\frac{3}{2}}}{3} \quad (5)$$

If the two particles are not in direct contact, the JKR model can provide attractive cohesion. At this time, the maximum gap between the two particles is:

$$\gamma_c = \frac{\alpha_c^2}{R^*} - \sqrt{\frac{4\pi U_S \alpha_c}{E^*}} \quad (6)$$

$$\alpha_c = \left[\frac{9\pi U_S R^*}{2E^*} - \left(\frac{3}{4} - \frac{1}{\sqrt{2}} \right) \right]^{\frac{1}{3}} \quad (7)$$

In the formula, γ_c is the maximum normal gap between particles with non-zero cohesion, mm; α_c is the maximum tangential gap when there is non-zero cohesion between particles, mm.

When the particles are in non-actual contact and the gap is less than or equal to γ_c, the cohesion of the JKR model reaches the maximum.

$$F_{pullout} = -\frac{3}{2}\pi U_S R^* \quad (8)$$

At this time, the adhesion between particles is in a critical state, and if the tension is increased, the two particles are separated. Therefore, the maximum tensile force F_l that separates the two particles is:

$$F_l = -\frac{3}{2}\pi U_S R^* \quad (9)$$

In order to accurately express the adhesion phenomenon, the Hertz-Mindlin with JKR contact model was selected to construct the quinoa seed-soil interaction model, and the discrete element parameters of the quinoa seed-soil mixture were calibrated.

(2) Shear Modulus Measurement

In this paper, the seeds of Mengli No.1 were selected for experiment. Because the seed size is small and the difference between the seeds is small, it is assumed that the seed size is the same in the simulation. The quinoa seeds were scanned and sampled by a three-dimensional scanner to obtain a quinoa seed model, which was imported into the EDEM simulation software for filling. This process yielded a quinoa seed model closely matching the real seed. The soil of quinoa planting area in Inner Mongolia was selected, and the soil was screened by 2 mm fine sieve to obtain soil particles with uniform particle size. A soil model was established using spherical particles in EDEM, as shown in Figure 3(a). In the dynamic angle of repose simulation test, the size of the rotating drum is consistent with the actual size, as shown in Figure 3(b). According to the literature, the parameters of this simulation are determined, as shown in Table 1. During the test, the particles are generated by the particle factory. After the particles reach a stable state, the drum rotates at a speed of 20 r/min.

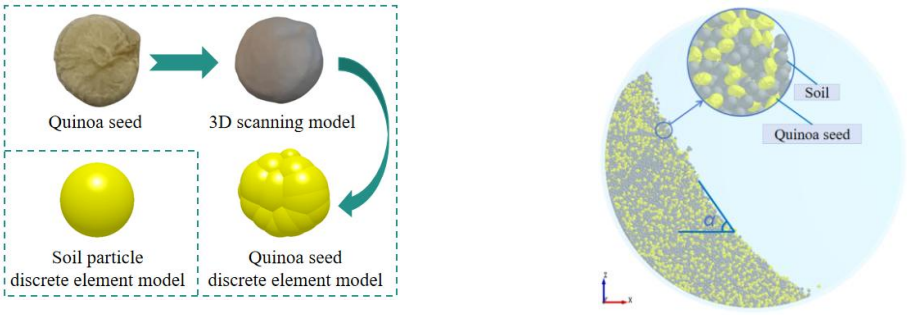

(a) **(b)**

Fig. 3 - Dynamic angle of repose simulation model

Table 1

Simulation parameter

Parameters	Numerical values
Poisson 's ratio of soil	0.46
Shear modulus of soil / Pa	4.3×10^{10}
Soil density / (g/cm^{-3})	2.65
Poisson 's ratio of quinoa	0.2
Shear modulus of quinoa / Pa	3.9×10^{8}
Quinoa density / (g/cm^{-3})	0.87
Poisson 's ratio of organic glass	0.37
Shear modulus of organic glass / Pa	2.3×10^{9}
Organic glass density / (g/cm^{-3})	1.15
Restitution coefficient of soil-organic glass collision	0.4
Quinoa seed-organic glass collision recovery coefficient	0.45
Quinoa seed-organic glass static friction coefficient	0.55
Dynamic friction coefficient of quinoa seed-organic glass	0.12

Based on the previous repeated experiments and the parameter selection range of reference (*Dong et al., 2023*), the variation range of quinoa seed-soil contact physical parameters was determined as shown in table 2.

Table 2

Discrete element simulation parameters

Factor	Level	
	-1	1
Quinoa seed-soil collision recovery coefficient *A*	0.2	0.6
Quinoa seed-soil static friction coefficient *B*	0.3	0.7
Quinoa seed-soil dynamic friction coefficient *C*	0.05	0.25
Soil-soil collision recovery coefficient *D*	0.2	0.6
Soil-soil static friction coefficient *E*	0.2	1
Soil-soil dynamic friction coefficient *F*	0.05	0.25
Soil-organic glass static friction coefficient *G*	0.3	0.9
Soil-organic glass dynamic friction coefficient *H*	0.05	0.25
Soil surface energy *I* / (J·m^2)	0.2	0.8
Quinoa seed-soil surface energy *J* / (J·m^2)	0.3	0.7

Plackett-Burman screening test was designed by Design-Expert software. The dynamic angle of repose of quinoa seed-soil mixture was used as the test index to screen out the parameters that had a significant impact on the index. On the basis of analyzing the results of Plackett-Burman screening test, the steepest ascent test was carried out on the selected factors with greater contribution. According to the principle of Box-Behnken test, the simulation parameters were calibrated and optimized. Finally, the dynamic angle of repose is measured by the image recognition method.

RESULTS

Analysis of Contact Between Quinoa Seeds and Soil

Figure 4 illustrates the load-displacement curve of quinoa seeds in contact with soil at three different moisture contents. In this figure, the x-axis represents the displacement of the seed caused by the probe, while the y-axis indicates the contact force between the quinoa seed and the soil. A negative contact force value signifies the bonding force between the quinoa seeds and soil during the upward movement of the seeds with the probe. The quinoa seeds were weighed using an electronic balance with an accuracy of 0.01 grams, with each seed's mass measured at 0.03 grams. The combined weight of six seeds was calculated to be 0.002 N. From Figure 4, it can be observed that when the soil moisture content is 15%, the maximum bonding force between the quinoa seeds and the soil is 0.051 N. At a soil moisture content of 17.5%, the maximum bonding force increases to 0.113 N. When the soil moisture content reaches 20%, the maximum bonding force further rises to 0.158 N. It is evident that the cohesive force between the quinoa seeds and the soil is significantly greater than the gravitational force acting on the seeds themselves. Therefore, when developing a contact model for quinoa seeds and soil, the adhesion between the seeds and soil must be taken into account.

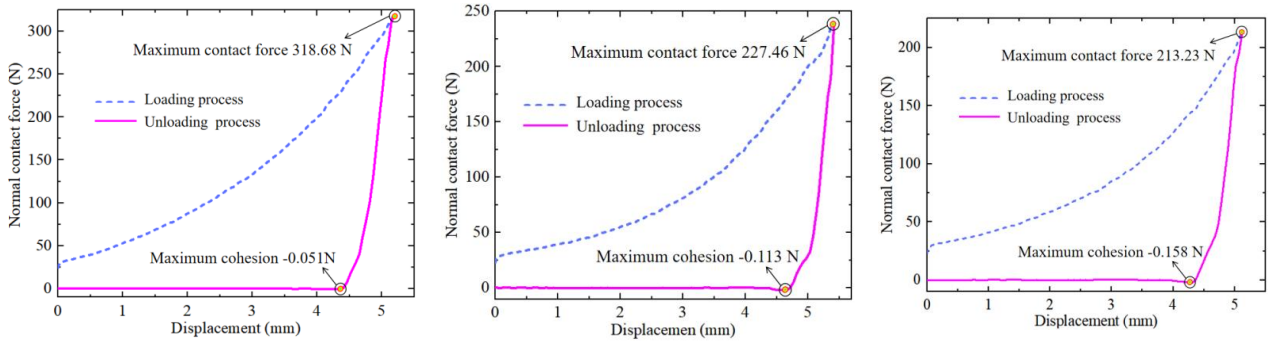

(**a**) (**b**) (**c**)

Fig. 4 - Load displacement curves under different water content

(a) The soil moisture content is 15%; (b) The soil moisture content is 17.5%; (c) The soil moisture content is 20%.

During the loading phase, the load-displacement curve resembles the non-viscous contact behavior described by the Hertz model. In contrast, during the unloading phase, the load-displacement curve follows a pattern similar to the Boussinesq linear relationship, particularly as the seed is about to detach from the soil surface, indicating a critical bonding point between the seed and the soil. Based on this observation, it is inferred that the JKR model could effectively describe the quinoa seed-soil contact interaction. Consequently, the Hertz-Mindlin model, incorporating the JKR contact mechanics, was selected to construct the quinoa seed-soil interaction model.

Physical Test Results of Quinoa Seed-soil Dynamic Angle of Repose

The physical test of the dynamic angle of repose of quinoa seed-soil mixture is shown in Figure 5. The test results are shown in Table 3. When the soil moisture content is in the range of 15% to 20%, the dynamic angle of repose increases as the soil moisture content rises.

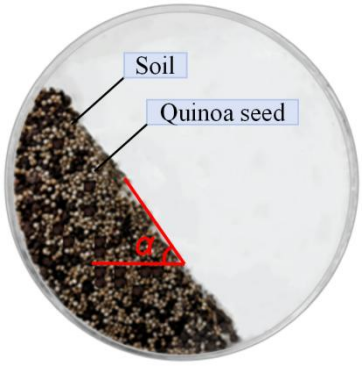

Fig. 5 - Physical test of dynamic angle of repose

Table 3

Physical test results of dynamic angle of repose

Moisture content / %	Dynamic angle of repose / (°)	Mean value
15	54.2 53.8 54.9	54.3
17.5	55.0 55.7 54.6	55.1
20	56.1 57.2 56.4	56.7

Simulated Test Results of Quinoa Seed-soil Dynamic Angle of Repose

(1) Plackett-Burman Test Results

The design and results of Plackett-Burman screening test are shown in Table 3. The Design-Expert software was used to process the data in Table 4, and the significant order of the influence of each parameter on the dynamic angle of repose was shown in Table 5.

Table 4

Results of response surface test

Test	Factor										Dynamic angle of repose / (°)
	A	*B*	*C*	*D*	*E*	*F*	*G*	*H*	*I*	*J*	
1	1	-1	1	1	-1	-1	-1	1	-1	1	55.5
2	-1	-1	-1	-1	-1	-1	-1	-1	-1	-1	48.3
3	1	-1	1	-1	1	1	1	-1	-1	-1	57.2
4	1	1	-1	1	1	1	-1	-1	-1	1	58.9
5	-1	-1	-1	1	-1	1	1	-1	1	1	64.7
6	-1	-1	1	-1	1	1	-1	1	1	1	69.9
7	1	-1	-1	1	1	-1	1	1	1	-1	58.1
8	-1	1	1	1	1	-1	-1	-1	1	-1	59.7
9	-1	1	1	1	-1	1	1	1	-1	-1	42.7
10	-1	1	-1	-1	1	-1	1	1	-1	1	46.8
11	1	1	1	-1	-1	-1	1	-1	1	1	61.5
12	1	1	-1	-1	-1	1	-1	1	1	-1	57.2

Table 5

Significance analysis of Plackett-Burman screening test results

Source of Variance	Sum of Squares	Freedom	Mean Square	*F*-Value	*P*-Value	Significance
Model	643.35	64.33	10	267.13	0.0476	*
A	22.14	22.14	1	91.93	0.0662	
B	60.30	60.30	1	250.38	0.0402	*
C	13.02	13.02	1	54.07	0.0861	
D	0.1408	0.1408	1	0.5848	0.5844	
E	35.71	35.71	1	148.27	0.0522	
F	35.71	35.71	1	148.27	0.0522	
G	28.52	28.52	1	118.43	0.0583	
H	33.67	33.67	1	139.80	0.0537	
I	317.24	317.24	1	1317.26	0.0175	*
J	96.90	96.90	1	402.36	0.0317	*
Residuals	0.2408	0.2408	1	267.13	0.0476	*
Cor Total	643.59		11			

According to the relevant data in Table 5, the Pareto diagram is drawn, as shown in Figure 6. It can be seen from Table 4 and Figure 7 that the significance of the influence of each contact parameter on the dynamic angle of repose is ranked from large to small: soil surface energy, quinoa seed-soil surface energy, quinoa seed-soil static friction coefficient, soil-soil static friction coefficient, soil-soil dynamic friction coefficient, soil-organic glass dynamic friction coefficient, soil-organic glass static friction coefficient, quinoa seed-soil collision recovery coefficient, quinoa seed-soil dynamic friction coefficient, soil-soil collision recovery coefficient. Among them, the three factors of soil surface energy, quinoa seed-soil surface energy and quinoa seed-soil static friction coefficient had significant effects, and the total contribution rate was 73.75%. The other seven factors were not significant. Therefore, three factors of soil surface energy, quinoa seed-soil surface energy and quinoa seed-soil static friction coefficient were selected for the steepest climbing test.

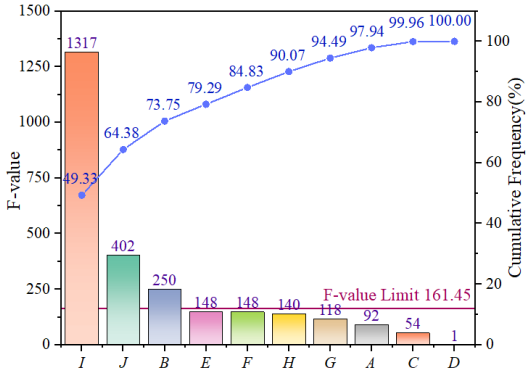

Fig. 6 - Pareto chart of PB design

(2) **Steepest climbing test Results**

Based on the analysis of the results of Plackett-Burman test, the steepest ascent test was carried out on the three significant factors. The relative error between the actual dynamic repose angle and the simulated dynamic repose angle is calculated to determine the optimal range of the simulation parameters. In the simulation process, the parameters that have no significant effect are removed from the intermediate level: Soil-soil static friction coefficient 0.6, soil-soil dynamic friction coefficient 0.15, soil-organic glass dynamic friction coefficient 0.15, soil-organic glass static friction coefficient 0.6, quinoa seed-soil collision recovery coefficient 0.4, quinoa seed-soil dynamic friction coefficient 0.15, soil-soil collision recovery coefficient 0.4.

The design and results of the steepest climbing test are shown in Table 6. The results show that the dynamic repose angle error is the smallest in the second group of tests, and the optimal interval can be determined near the second group of parameter values. Therefore, the Box-Behnken test was carried out with the second group of parameter values as the intermediate level, and the third group of parameter values of the first group as the low level and the high level respectively.

Table 6

Steepest climbing test design and results

Test	Soil surface energy / (J·m^2)	Quinoa seed-soil surface energy / (J·m^2)	Quinoa seed-soil static friction coefficient	Dynamic angle of repose / (°)	Relative error / %
1	0.3	0.2	0.3	52.6	-4.5
2	0.4	0.35	0.4	56.4	2.4
3	0.5	0.5	0.5	60.1	8.1
4	0.6	0.65	0.6	64.3	16.7
5	0.7	0.8	0.7	69.4	26.0

(3) **Box-Behnken Test Results**

In order to find the optimal parameter combination of soil surface energy, quinoa seed-soil surface energy and quinoa seed-soil static friction coefficient in the simulation test. Based on the steepest climbing test, the dynamic angle of repose was used as the test index, and the three-factor three-level response surface test was carried out according to the Box-Behnken test principle. The experimental design and results are shown in Table 7.

Table 7

Box-Behnken experimental design and results

Test	Factor			Dynamic angle of repose *Y* / (°)
	I	*J*	*B*	
1	-1	0	1	53.1
2	0	0	0	54.6
3	-1	-1	0	52.4
4	-1	1	0	56.1
5	0	0	0	55.7
6	-1	0	-1	53.6
7	1	0	-1	54.2
8	0	-1	1	53.7

Test	Factor			Dynamic angle of repose *Y* / (°)
	I	*J*	*B*	
9	0	-1	-1	54.1
10	1	1	0	60.3
11	1	0	1	58.9
12	1	-1	0	54.7
13	0	1	1	58.6
14	0	0	0	55.3
15	0	1	-1	56.2
16	0	0	0	55.6
17	0	0	0	54.9

The regression analysis of the test results was carried out by Design-Expert software, as shown in Table 8, and the regression equation of the qualified rate *Y* was obtained:

$$Y = 55.22 + 1.61I + 2.04J + 0.775B + 0.475IJ + 1.3IB + 0.7JB - 0.0225I^2 + 0.6775J^2 - 0.2475B^2 \quad (10)$$

Table 8

Analysis of variance

Source of Variance	Sum of Squares	Mean Square	Freedom	*F*-Value	*P*-Value	Significance
Model	70.56	9	7.84	25.70	0.0001	**
I	20.80	1	20.80	68.18	< 0.0001	**
J	33.21	1	33.21	108.86	< 0.0001	**
B	4.81	1	4.81	15.75	0.0054	**
IJ	0.9025	1	0.9025	2.96	0.1291	
IB	6.76	1	6.76	22.16	0.0022	**
JB	1.96	1	1.96	6.42	0.0390	*
I^2	0.0021	1	0.0021	0.0070	0.9357	
J^2	1.93	1	1.93	6.34	0.0400	*
B^2	0.2579	1	0.2579	0.8454	0.3884	
Residuals	2.14	7	0.3051			
Lack of fit	1.27	3	0.4225	1.95	0.2639	
Pure error	0.8680	4	0.2170			
Cor total	72.70	16				

It can be seen from the results of variance analysis that the three factors of soil surface energy, quinoa seed-soil surface energy and quinoa seed-soil static friction coefficient have extremely significant effects on the dynamic angle of repose, and some factors have pairwise interactions. The regression model fitting degree of the evaluation index was extremely significant, and the lack of fit item $P > 0.05$, indicating that there were no other factors affecting the evaluation index. Through the regression coefficient test, the primary and secondary order of the factors affecting the dynamic angle of repose is quinoa seed-soil surface energy *J*, soil surface energy *I* and quinoa seed-soil static friction coefficient *B*.

According to the regression equation, the surface diagram of the influence of the factors with significant interaction on the evaluation index is drawn, as shown in Figure 7. From Figure 7(a), it can be seen that compared with quinoa seed-soil surface energy *J*, the soil surface energy *I* curve is steeper, indicating that it has a more significant impact on the dynamic angle of repose. It can be seen from Figure 7(b) that the soil surface energy *I* is similar to the trend of the quinoa seed-soil static friction coefficient *B* curve, indicating that the two factors have a more significant effect on the dynamic angle of repose. It can be seen from Figure 7(c) that compared with the quinoa seed-soil surface energy *J*, the quinoa seed-soil static friction coefficient *B* curve is steeper, indicating that it has a more significant effect on the dynamic angle of repose.

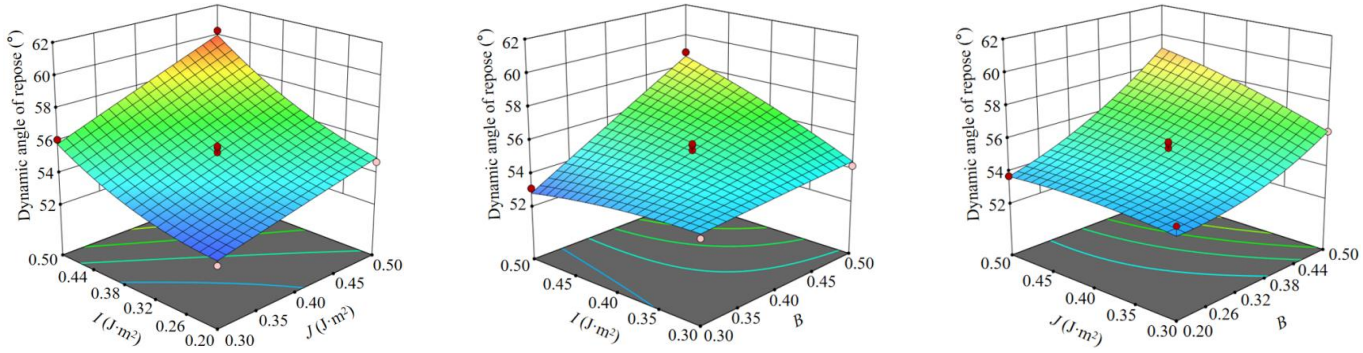

(a) (b) (c)

Fig. 7 - The effect of interaction on dynamic angle of repose

(4) Parameter Optimization and Simulation Verification Results

In order to obtain the best combination of parameters, the optimization module of Design-Expert software was used to optimize the analysis within the range of factor levels with 54.3°, 55.1° and 56.7° as the target values. The optimal parameter combination was determined. When the soil moisture content was 15%, the soil surface energy was 0.351 J·m^2, the quinoa seed-soil surface energy was 0.347 J·m^2, and the quinoa seed-soil static friction coefficient was 0.489. When the soil moisture content was 17.5%, the soil surface energy was 0.343 J·m^2, the quinoa seed-soil surface energy was 0.409 J·m^2, and the quinoa seed-soil static friction coefficient was 0.400. When the soil moisture content was 20%, the soil surface energy was 0.473 J·m^2, the quinoa seed-soil surface energy was 0.354 J·m^2, and the quinoa seed-soil static friction coefficient was 0.415.

The optimized parameters were used for verification test. The verification test results are shown in Figure 8, and the errors with the physical test are -1.8%, 0.9%, and 1.9%, respectively. The error is small, which proves the accuracy of the calibration parameters.

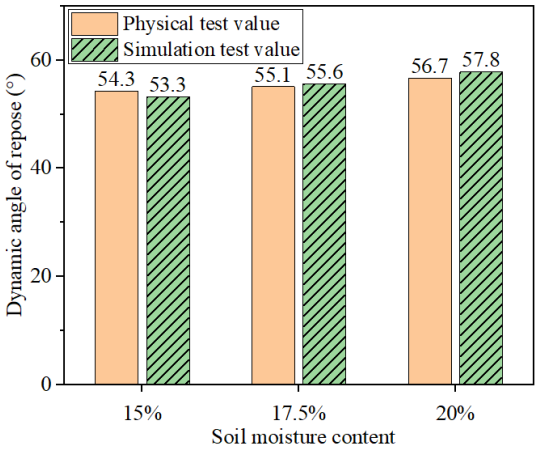

Fig. 8 - Comparison diagram of verification test and physical test

DISCUSSION

In recent years, as the discrete element (DEM) simulation is not limited by seasonal climate, more and more scholars use simulation to simulate the seeding process (*Tang et al., 2022; Luo et al., 2023*). The biggest difficulty of using DEM simulation is to select the correct model and the corresponding contact parameters (*Chen et al., 2023*). In this study, the contact process between quinoa seeds and soil under different soil water contents was analyzed by contact test. In the loading process, the load-displacement curve is similar to the non-viscous contact relationship of Hertz model. During the unloading process, the load-displacement curve is similar to the Boussinesq linear relationship when the seed is about to leave the soil surface to the critical bonding between the seed and the soil. This is consistent with the theoretical analysis results of Borodich, F.M.et al. (*Borodich et al., 2014*) JKR model. Compared with the load-displacement curve of the EEPA model, the load-displacement curve of the contact test is closer to the load-displacement curve of the JKR model, as shown in Figure 9. Therefore, the JKR model was selected as the quinoa seed-soil contact model. According to the agronomic requirements of quinoa planting, the soil moisture content should be between 15% and 20%. Therefore, it is of practical significance to select the soil moisture content range of 15% -20%.

In this range, the adhesion of soil to quinoa seeds increased with the increase of soil moisture content, which was consistent with the results of Zhou et al. (*Zhou et al., 2023*). In the process of sowing, it can be considered to appropriately increase the soil moisture content and increase the adhesion of the soil to the seed to reduce the bounce of the seed and the soil, thereby improving the uniformity of sowing.

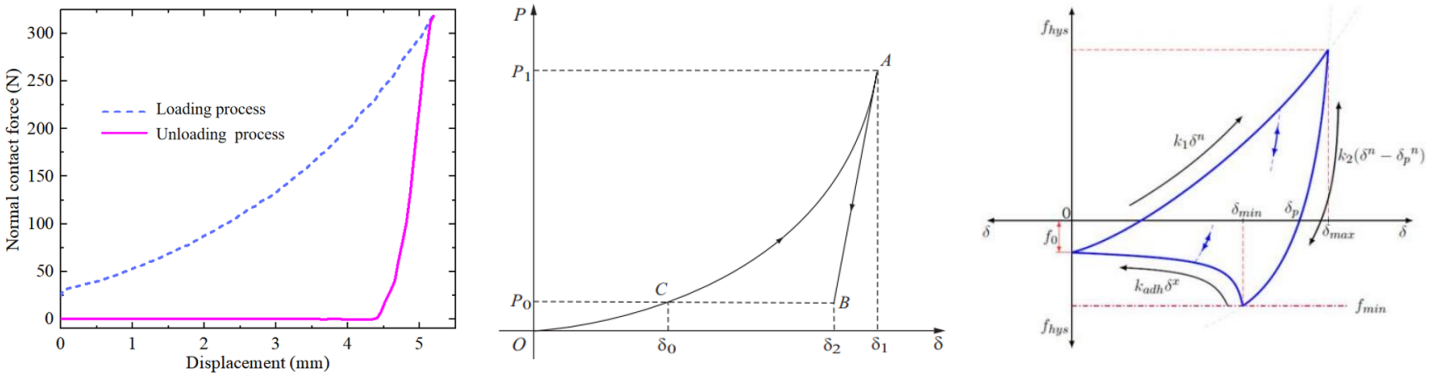

(a) (b) (c)

Fig. 9 - Load displacement curve comparison diagram

(Zhou et al., 2023; Borodich et al., 2014)

(a) Load-displacement curve of contact test; (b) Load-displacement curve of JKR model; (c) Load-displacement curve of EEPA model.

At present, the calibration of discrete element simulation parameters mostly uses static angle of repose as a macro index (*Fang et al., 2022; Shi et al., 2022*). In the seeding operation, when the seed collides with the soil, most of the soil particles are in a moving state under the action of the opener, and the static angle of repose is not enough to fully characterize the rheological properties of the soil. Therefore, this paper chooses the dynamic angle of repose as the macro index. In the physical experiment of dynamic angle of repose, the dynamic angle of repose increases with the increase of soil moisture content. Seeds and soil particles are difficult to separate due to adhesion. The greater the adhesion is, the more difficult it is to separate, and the greater the dynamic angle of repose is. *Zhou et al.* (*2023*) concluded that the angle of repose does not increase with the increase of soil moisture content. There are two main reasons for the differences in the conclusions. First, the macro indicators are different. In this paper, the dynamic angle of repose is used as the macro indicator, and *Zhou Long et al.* used the static angle of repose as the macro indicator, as shown in Figure 10. Secondly, the range of sudden moisture content is different. The range of soil moisture content in this paper is 15% -20%, and the range of soil moisture content such as Zhou long is 15% -25%. In the static angle of repose test, when the soil moisture content exceeds 20%, the larger adhesion force of the soil to the seeds prevents the free scattering of particles, and the angle of repose formed by direct collapse in the final stage is smaller. In the dynamic angle of repose test, the seeds and soil particles rotate uniformly in the drum, avoiding the occurrence of sudden collapse.

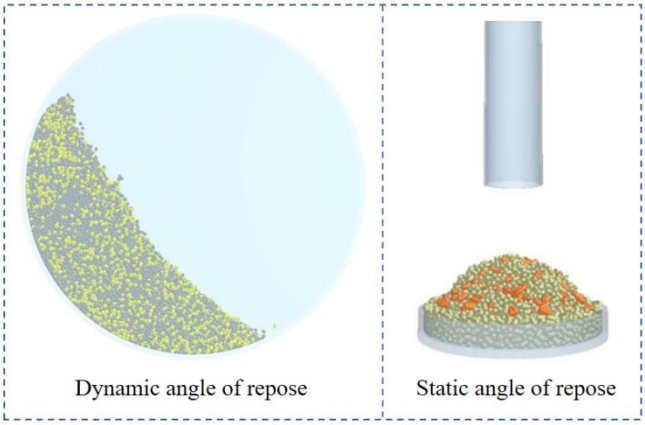

Fig. 10 - Comparison of dynamic static angle of repose (Zhou et al., 2023)

By comparing the calibration results of different scholars' JKR model parameters, it is found that the particle surface energy has a significant effect on the test index (*Qiu et al., 2022; Zeng et al., 2023*). In this study, the Plackett-Burman test was used to screen out the factors that had a significant effect on the dynamic

angle of repose, which were soil surface energy, quinoa seed-soil surface energy, and quinoa seed-soil static friction coefficient. Based on the analysis and optimization of Box-Behnken test, the optimal parameter combination under different water content was determined. Compared with the physical test results, the error was within 1.9%. This proves the feasibility and accuracy of the JKR model as a quinoa seed-soil mixture contact model.

CONCLUSIONS

This study investigated the contact process between seeds and soil. The adhesion force of the soil to the seeds is significantly greater than the seeds' own force, and it increases with the soil's moisture content. The load-displacement curves obtained from the experiments are similar to those of the JKR (Johnson-Kendall-Roberts) adhesion model. Consequently, the JKR model is deemed suitable for use as a discrete element model for seeds with small diameters, such as quinoa, interacting with soil mixtures.

Through a physical experiment measuring the dynamic angle of repose, it was observed that the dynamic angle of repose increases as the soil moisture content increases.

The Plackett-Burman test was designed by Design-Expert software using the method of combining physical test and simulation test. The factors that significantly affected the dynamic angle of repose were soil surface energy, quinoa seed-soil surface energy and quinoa seed-soil static friction coefficient. Through the Box-Behnken test, a second-order regression model between the dynamic angle of repose and the three factors was established and the variance and regression model interaction effects were analyzed. The influence parameters are optimized to obtain the best parameter combination. When the soil moisture content was 15%, the soil surface energy was 0.351 J·m^2, the quinoa seed-soil surface energy was 0.347 J·m^2, and the quinoa seed-soil static friction coefficient was 0.489. When the soil moisture content was 17.5%, the soil surface energy was 0.343 J·m^2, the quinoa seed-soil surface energy was 0.409 J·m^2, and the quinoa seed-soil static friction coefficient was 0.400. When the soil moisture content was 20%, the soil surface energy was 0.473 J·m^2, the quinoa seed-soil surface energy was 0.354 J·m^2, and the quinoa seed-soil static friction coefficient was 0.415.

ACKNOWLEDGEMENT

This work was funded by The National Natural Science Foundation of China (32060418), The National Key Research and Development Program of China (2023YFD1600701), Inner Mongolia Autonomous Region Science and Technology Planning Project (2023YFDZ0024), Inner Mongolia Autonomous Region Science and Technology Planning Project (2025YFHH0133), Inner Mongolia Autonomous Region 'first-class discipline scientific research special project' (YLXKZX-NND-046) and Key R & D project of Ordos City (YF20232341).

REFERENCES

[1] Abdolahzare, Z., & Mehdizadeh, S. A. (2018). Real time laboratory and field monitoring of the effect of the operational parameters on seed falling speed and trajectory of pneumatic planter. *Computers and Electronics in Agriculture*, 145, 187-198. https://doi.org/10.1016/j.compag.2018.01.001.

[2] Borodich, F. M., Galanov, B. A., Keer, L. M., & Suarez-Alvarez, M. M. (2014). The JKR-type adhesive contact problems for transversely isotropic elastic solids. *Mechanics of Materials*, 75, 34-44. http://dx.doi.org/10.1016/j.mechmat.2014.03.011.

[3] Cay, A., Kocabiyik, H., & May, S. (2018). Development of an electro-mechanic control system for seed-metering unit of single seed corn planters Part I: Design and laboratory simulation. *Computers and Electronics in Agriculture*, 144, 71-79. https://doi.org/10.1016/j.compag.2017.11.035.

[4] Chen, X., Gu, F., Hu, Z., Wu, F., Luo, W., & Guo, K. (2023). The calibration of soil simulation parameters for wheat grown after rice in the Yangtze River Basin of China. *Sustainability*, 15(15079). https://doi.org/10.3390/su152015079.

[5] Dong, W. X., Li, N., Liu, F., Zhao, X., Wang, L. H., Xuan, D. Z., Zhong, W. D., Hu, H. T., Kong, X., Meng, X. Y., & Li, M. Y., Duan, Z. J. (2023). Study on vibration adsorption characteristics of small particle size seeds based on DEM. *INMATEH-Agricultural Engineering*, 71(3). https://doi.org/10.35633/inmateh-71-35.

[6] Fang, M., Yu, Z. H., Zhang, W. J., Gao, J., & Liu, W. H. (2022). Friction coefficient calibration of corn stalk particle mixtures using Plackett-Burman design and response surface methodology. *Powder Technology*, 396, 731-742. https://doi.org/10.1016/j.powtec.2021.10.040.

[7] Fang, W., Wang, X., Han, D., & Chen, X. (2022). Review of material parameter calibration method. *Agriculture*, 12(706). https://doi.org/10.3390/agriculture12050706.

[8] Horabik, J., Wiacek, J., Parafiniuk, P., Banda, M., Kobylka, R., & Stasiak, M., & Molenda, M. (2020). Calibration of discrete-element-method model parameters of bulk wheat for storage. *Biosystems Engineering*, 200, 298-314. https://doi.org/10.1016/j.biosystemseng.2020.10.010.

[9] Jiang, D., Chen, X., Yan, L., Gou, H., Yang, J., & Li, Y. (2023). Parameter calibration of discrete element model for cotton rootstalk-soil mixture at harvest stage in Xinjiang cotton field. *Agriculture*, 13(1344). https://doi.org/10.3390/agriculture13071344.

[10] Lei, X. L., Hu, H. J., Wu, W. C., Liu, H. N., Liu, L. Y., Yang, W. H., Zhou, Z. L., & Ren, W. J. (2021). Seed motion characteristics and seeding performance of a centralised seed metering system for rapeseed investigated by DEM simulation and bench testing. *Biosystems Engineering*, 203, 22-33. https://doi.org/10.1016/j.biosystemseng.2020.12.017.

[11] Li, S. P., Pan, J. F., Zhong, J. Q., Huang, Z. X., & Gan, F. F. (2022). Design and experiment of furrow opener for transversal sugarcane planter based on effective seeding space. *Transactions of the Chinese Society for Agricultural Machinery*, 53(7), 162-170. https://doi.org/10.6041/j.issn.1000-1298.2022.07.016.

[12] Liao, Y. Y., You, Y., Wang, D. C., Zhang, X. N., Zhang, H. F., & Ma, W. P. (2022). Parameter calibration and experiment of discrete element model for mixed seeds of oat and arrow pea. *Transactions of the Chinese Society for Agricultural Machinery*, 53(8), 14-22. https://doi.org/10.6041/j.issn.1000-1298.2022.08.002.

[13] Liao, Y., You, Y., Hui, Y., Zhang, X., & Wang, D. (2023). Mixed seeds of oat and vetch based on DEM-Fluent coupling motion simulation in a Venturi tube. *Processes*, 11(1095). https://doi.org/10.3390/pr11041095.

[14] Liu, R., Liu, L., Li, Y., Liu, Z., Zhao, J., Liu, Y., & Zhang, X. (2022). Numerical simulation of seed-movement characteristics in new maize delivery device. *Agriculture*, 12(1944). https://doi.org/10.3390/agriculture12111944.

[15] Liu, R., Li, Y. J., Liu, Z. J., Liu, L. J., & Lv, H. T. (2021). Analysis and calibration of discrete element parameters of coated maize seed. *Transactions of the Chinese Society for Agricultural Machinery*, 52(S1), 1-8+18. https://doi.org/10.6041/j.issn.1000-1298.2021.S0.006.

[16] Luo, W., Chen, X., Guo, K., Qin, M., Wu, F., Gu, F., & Hu, Z. (2023). Optimization and accuracy analysis of a soil–planter model during the sowing period of wheat after a rice stubble based discrete element method. *Agriculture*, 13(2036). https://doi.org/10.3390/agriculture13102036.

[17] Ma, X. J., Liu, M., Hou, Z., Li, J., Gao, X., Bai, Y., & Guo, M. (2022). Calibration and experimental studies on the mixing parameters of red clover seeds and coated powders. *Processes*, 10(2280). https://doi.org/10.3390/pr10112280.

[18] Pareek, C. M., Tewari, V. K., & Brajesh, N. (2023). A mechatronic seed metering control system for improving sowing uniformity of planters. *Journal of Engineering Research*. Available online 3 November 2023. https://doi.org/10.1016/j.jer.2023.10.041.

[19] Qiu, Y., Guo, Z., Jin, X., Zhang, P., Si, S., & Guo, F. (2022). Calibration and verification test of cinnamon soil simulation parameters based on discrete element method. *Agriculture*, 12(1082). https://doi.org/10.3390/agriculture12081082.

[20] Shi, G., Li, J., Ding, L., Zhang, Z., Ding, H., Li, N., & Kan, Z. (2022). Calibration and tests for the discrete element simulation parameters of fallen jujube fruit. *Agriculture*, 12(38). https://doi.org/10.3390/agriculture12010038.

[21] Shi, L., Zhao, W., Rao, G., Guo, J., & Wang, Z. (2023). Modeling of typically shaped corn seeds and calibration of the coefficient of rolling friction. *Agronomy*, 13(1573). https://doi.org/10.3390/agronomy13061573.

[22] Song, Z. H., Li, H., Yan, Y. F., Tian, F. Y., Li, Y. D., & Li, F. D. (2022). Calibration method of contact characteristic parameters of soil in mulberry field based on unequal-diameter particles DEM theory. *Transactions of the Chinese Society for Agricultural Machinery*, 53(6), 21-33. https://doi.org/10.6041/j.issn.1000-1298.2022.06.002.

[23] Sun, K., Yu, J. Q., Liang, L. S., Wang, Y., Yan, D. X., Zhou, L., & Yu, Y. J. (2022). A DEM-based general modelling method and experimental verification for wheat seeds. *Powder Technology*, 401, 117353. https://doi.org/10.1016/j.powtec.2022.117353.

[24] Sun, J., Zhang, Y., Zhang, Y., Li, P., & Teng, G. (2022). Precision seeding compensation and positioning based on multisensors. *Sensors*, 22(7228). https://doi.org/10.3390/s22197228.

[25] Tang, H., Xu, F. D., Xu, C. S., Zhao, J. L., & Wang, Y. J. (2023). The influence of a seed drop tube of the inside-filling air-blowing precision seed-metering device on seeding quality. *Computers and Electronics in Agriculture*, 204(107555). https://doi.org/10.1016/j.compag.2022.107555.

[26] Tian, X. L., Cong, X., Qi, J. T., Guo, H., Li, M., & Fan, X. H. (2021). Parameter calibration of discrete element model for corn straw-soil mixture in black soil areas. *Transactions of the Chinese Society for Agricultural Machinery*, 52(10), 100-108+242. https://doi.org/10.6041/j.issn.1000-1298.2021.10.010.

[27] Wang, X. L., Zhong, X. K., Geng, Y. L., Wei, Z. C., Hu, H., Geng, D. Y., & Zhang, X. C. (2021). Construction and parameter calibration of the nonlinear elastoplastic discrete element model for no-tillage soil compaction. *Transactions of the Chinese Society of Agricultural Engineering*, 37(23), 100-107. https://doi.org/10.11975/j.issn.1002-6819.2021.23.012.

[28] Wang, Y. X., Liang, Z. J., Zhang, D. X., Cui, T., Shi, S., Li, K. H., & Yang, L. (2016). Calibration method of contact characteristic parameters for corn seeds based on EDEM. *Transactions of the Chinese Society of Agricultural Engineering*, 32(22), 36-42. https://doi.org/10.11975/j.issn.1002-6819.2016.22.005.

[29] Walunj, A., Chen, Y., Tian, Y., & Zeng, Z. (2023). Modeling soil–plant–machine dynamics using discrete element method: A review. *Agronomy*, 13(1260). https://doi.org/10.3390/agronomy13051260.

[30] Xie, C., Zhang, D., Yang, L., Cui, T., He, X., Du, Z., & Xiao, T. (2023). Research and analysis on the influence of different speed measurement methods on the monitoring accuracy of seed spacing. *Agriculture*, 13(128). https://doi.org/10.3390/agriculture13010128.

[31] Yan, B. X., Wu, G. W., Fu, W. Q., Gao, N. N., Meng, Z. J., & Zhu, P. (2020). Influencing factors of corn implantation distribution for high-height planting based on EDEM. *Transactions of the Chinese Society for Agricultural Machinery*, 51(S2), 47-54. https://doi.org/10.6041/j.issn.1000-1298.2020.S2.006.

[32] Yang, L., Li, J. W., Lai, Q. H., Zhao, L. L., Li, J. J., Zeng, R. H., & Zhang, Z. H. (2024). Discrete element contact model and parameter calibration for clayey soil particles in the Southwest hill and mountain region. *Journal of Terramechanics*, 111, 73-87. https://doi.org/10.1016/j.jterra.2023.10.002.

[33] Yu, Q. X., Liu, Y., Chen, X. B., Sun, K., & Lai, Q. H. (2020). Simulation parameter calibration and experiment of Panax notoginseng seeds based on discrete element. *Transactions of the Chinese Society for Agricultural Machinery*, 51(2), 123-132. https://doi.org/10.6041/j.issn.1000-1298.2020.02.014.

[34] Zeng, Y., Chen, C., Quan, W., Xie, S., Shi, F., Ma, Z., & Wu, M. (2023). Calibration parameter of soil discrete element based on area difference method. *Agriculture*, 13(648). https://doi.org/10.3390/agriculture13030648.

[35] Zhang, R. F., Jiao, W., Zhou, J. L., Qi, B., Liu, H., & Xia, Q. Q. (2020). Parameter calibration and experiment of rice seeds discrete element model with different filling particle radius. *Transactions of the Chinese Society for Agricultural Machinery*, 51(S1), 227-235. https://doi.org/10.6041/j.issn.1000-1298.2020.S1.026.

[36] Zhang, S., Yang, F., Dong, J., Chen, X., Liu, Y., Mi, G., Wang, T., Jia, X., Huang, Y., & Wang, X. (2022). Calibration of discrete element parameters of maize root and its mixture with soil. *Processes*, 10(2433). https://doi.org/10.3390/pr10112433.

[37] Zhao, L., Zhou, H. P., Xu, L. Y., Song, S. Y., Zhang, C., & Yu, Q. X. (2022). Parameter calibration of coconut bran substrate simulation model based on discrete element and response surface methodology. *Powder Technology*, 395, 183-194. https://doi.org/10.1016/j.powtec.2021.09.065.

[38] Zhou, L., Dong, Q., Yu, J., Wang, Y., Chen, Y., Li, M., Wang, W., Yu, Y., & Yuan, J. (2023). Validation and calibration of maize seed-soil inter-parameters based on the discrete element method. *Agronomy*, 13(2115). https://doi.org/10.3390/agronomy13082115.

[39] Zhou, H., Chen, H. L., Geng, D. Y., Chen, M. Z., & Zhang, M. P. (2023). Discrete element modeling and parameter calibration of typical soil in maize field tillage layer. *Transactions of the Chinese Society for Agricultural Machinery*, 54(11), 49-60+113. https://doi.org/10.6041/j.issn.1000-1298.2023.11.005.